RAPID COMMUNICATION

Spin reorientation in easy-plane kagome ferromagnet $Li_9Cr_3(P_2O_7)_3(PO_4)_2$

Yuanhao Dong(董元浩)[1], Ying Fu(付盈)[2], Yixuan Liu(刘以轩)[3], Zhanyang Hao(郝占阳)[3], Le Wang(王乐)[1], Cai Liu(刘才)[1], Ke Deng(邓可)[1], and Jiawei Mei(梅佳伟)[1,4,†]

[1] *Shenzhen Institute for Quantum Science and Engineering, and Department of Physics, Southern University of Science and Technology, Shenzhen* 518055, *China*
[2] *School of Physics, Xi'an Jiaotong University, Xi'an* 710049, *China*
[3] *Department of Physics, Southern University of Science and Technology, Shenzhen* 518055, *China*
[4] *Shenzhen Key Laboratory of Advanced Quantum Functional Materials and Devices, Southern University of Science and Technology, Shenzhen* 518055, *China*

(Received 8 December 2022; revised manuscript received 21 February 2023; accepted manuscript online 9 March 2023)

We report the successful growth and characterization of $Li_9Cr_3(P_2O_7)_3(PO_4)_2$ single crystal, and investigate its magnetic properties under external magnetic fields via magnetization and heat capacity measurements. Our study reveals that $Li_9Cr_3(P_2O_7)_3(PO_4)_2$ is an easy-plane kagome ferromagnet with $S = 3/2$, as evidenced by the Curie–Weiss temperature of 6 K which implies a ferromagnetic exchange coupling in the material. Under zero magnetic field, $Li_9Cr_3(P_2O_7)_3(PO_4)_2$ undergoes a magnetic transition at $T_C = 2.7$ K from a paramagnetic state to a ferromagnetically ordered state with the magnetic moment lying in the kagome plane. By applying a c-axis directional magnetic field to rotate the spin alignment from the kagome plane to the c-axis, we observe a reduction in the magnetic transition temperature as the field is increased. We construct a magnetic phase diagram as a function of temperature and magnetic field applied parallel to the c-axis of $Li_9Cr_3(P_2O_7)_3(PO_4)_2$ and find that the phase boundary is linear over a certain temperature range. Regarding that theoretically, the field-induced phase transition of the spin reorientation in the easy-plane ferromagnet can be viewed as the ferromagnetic magnon Bose–Einstein condensation (BEC), the phase boundary scaling of field-induced ($B \parallel c$) magnetic transition in $Li_9Cr_3(P_2O_7)_3(PO_4)_2$ can be described as the quasi-2D magnon BEC, which has been observed in other ferromagnetic materials such as K_2CuF_4.

Keywords: kagome lattice, flux method, magnetic material, spin-3/2

PACS: 75.40.Cx, 06.60.Ei, 61.05.cp, 67.85.Jk **DOI:** 10.1088/1674-1056/acc2b3

1. Introduction

The kagome lattice is a well-established model for investigating the interplay between various physical properties, such as frustration, topology, and correlations, and has been extensively studied in literature.[1–4] $Li_9M_3(P_2O_7)_3(PO_4)_2$ (M = Al, Ga, Cr, Fe, etc.) is a compound whose lattice structure for the transition-metal ions is equivalent to a regular kagome lattice, considering only nearest-neighbor interactions.[5] These compounds have garnered interest among researchers in the field of electrochemistry as an ideal candidate material for lithium battery electrodes.[6–9] Its unique kagome lattice structure has made it a subject of study for exploring interplay among various physical properties, with recent findings shedding light on its magnetic and transport properties.[5,10,11] Some researchers reported on the low-temperature magnetism of $Li_9Fe_3(P_2O_7)_3(PO_4)_2$ ($S = 5/2$), which exhibits an antiferromagnetic long-range order developing at T_N = 1.3 K and a crossover from a paramagnet to a classical spin-liquid phase at approximately 5 K.[10] Additionally, the weak magnetic interaction allows for the observation of the 1/3 magnetization plateau under a stable field near $B = 4.75$ T, providing valuable opportunities to explore classical and quantum fluctuations effects with zero and applied fields of the Heisenberg antiferromagnetic model. Another material in this family, $Li_9V_3(P_2O_7)_3(PO_4)_2$ ($S = 1$), exhibits distinct properties.[11] The material's magnetic susceptibility measurements revealed a ferromagnetic Curie–Weiss temperature of 3 K and a lack of long-range magnetic order at low temperatures. Researchers attributed this observation to the XXZ model with single-ion uniaxial anisotropy.[11–14]

The magnetic properties of $Li_9Cr_3(P_2O_7)_3(PO_4)_2$ ($S = 3/2$), another member of this family, have fewer reports to date. In this work, we grew millimeter-scale single crystal samples of $Li_9Cr_3(P_2O_7)_3(PO_4)_2$ using the flux method to measure its magnetism and specific heat. We studied the effect of magnetic anisotropy and spin reorientation in the kagome lattice material $Li_9Cr_3(P_2O_7)_3(PO_4)_2$. Our experiments showed that $Li_9Cr_3(P_2O_7)_3(PO_4)_2$ is an easy-plane kagome ferromagnetic material with a spin of $S = 3/2$. We applied a c-axis directional field to rotate the spin alignment from the kagome plane to the c-axis and found that

[†]Corresponding author. E-mail: meijw@sustech.edu.cn

© 2023 Chinese Physical Society and IOP Publishing Ltd

the magnetic transition temperature decreased with increasing field. We then presented the phase diagram for temperature versus the magnetic field applied parallel to the c axis of $Li_9Cr_3(P_2O_7)_3(PO_4)_2$ and found that the phase boundary was linear over a certain temperature range. Theoretically, some researchers concluded that the magnetic field-induced transverse ordering could be understood as the Bose–Einstein condensation (BEC) of the lattice bosons. [15] Our findings are in agreement with the theory of quasi-2D Bose–Einstein condensation, as observed in the ferromagnetic material K_2CuF_4.[16]

2. Experimental methods

We grew millimeter-scale single crystal samples of $Li_9Cr_3(P_2O_7)_3(PO_4)_2$ using a flux method. The process involved mixing Li_3PO_4 (99%, Aladdin), Cr_2O_3 (99.96%, Alfa Aesar), and $(NH_4)_2HPO_4$ (99%, Aladdin) in a ratio of 10:1:10, grinding the mixture in an agate mortar, and heating it in a platinum crucible. After preheating at 400 °C for 10 h and then heating to 980 °C for 10 h, the product was cooled uniformly to 650 °C over 150 h and rapidly cooled to room temperature over 3 h. The resulting product contained two impurity phases, $Li_4P_2O_7$ and $LiPO_3$, which needed to be treated. We put the product into a 1 mol/L CH_3COOH solution and placed it on a heating table at 120 °C for 5 h to dissolve the $Li_4P_2O_7$. In the last step, we put the filtered solid into a saturated NaCl solution for 3 h. $LiPO_3$ becomes water-soluble $NaPO_3$ through Na–Li ion exchange. The water-insoluble solids that remained after filtration were the pure target single-crystal samples. Recently, we note that Akshata Magar's team had recently studied $Li_9Cr_3(P_2O_7)_3(PO_4)_2$ for its magnetocaloric effect and magnetic refrigeration applications.[17]

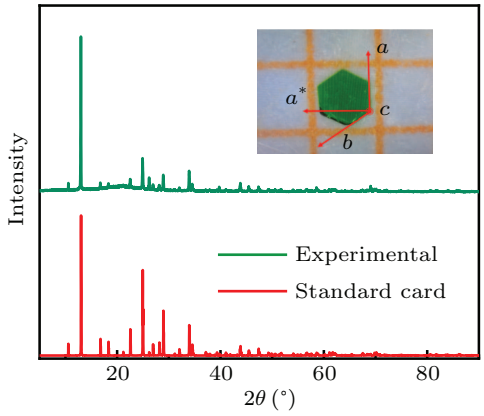


Fig. 1. Powder x-ray diffraction patterns (the inset is a photograph of the single-crystal $Li_9Cr_3(P_2O_7)_3(PO_4)_2$).

The resulting single crystal samples $Li_9Cr_3(P_2O_7)_3(PO_4)_2$ had sizes between 1 mm and 2 mm and appeared dark green in color with a relatively regular hexagonal platelet morphology. We used the Rigaku Smartlab-9 diffractometer to obtain x-ray powder diffraction (XRPD) patterns at 300 K with a scanning step width of 0.01° in the range of 5°–90°. The obtained data was compared with the standard card to determine the phase, as shown in Fig. 1. We measured the magnetic properties and specific heat of the samples using the magnetic property measurement system (MPMS) and physical property measurement system (PPMS) produced by Quantum Design (QD), respectively.

3. Results

3.1. Crystal structure

The crystal structure of $Li_9Cr_3(P_2O_7)_3(PO_4)_2$ is shown in Fig. 2(a), with space group $P\bar{3}c1$ and lattice constants $a = b = 9.666(1)$ Å and $c = 13.588(1)$ Å (in the hexagonal basis).[5] Similar to other members of this family such as $Li_9Fe_3(P_2O_7)_3(PO_4)_2$ and $Li_9V_3(P_2O_7)_3(PO_4)_2$, it has a triangular lattice with a $[(CrP_2O_7)_3(PO_4)_2]$ layered structure in the ab-plane. The structure is composed of CrO_6 octahedra sharing corners with P_2O_7 groups and PO_4 tetrahedra.[18,19]

As shown in Fig. 2(b), Cr^{3+} ions are arranged in an equilateral triangle within the intralayer. Although the distorted hexagon formed in the center loses rotational symmetry, the equilateral triangle-sharing angle network of Cr^{3+} is topologically equivalent to the regular kagome network if we only consider the nearest-neighbor magnetic coupling in the ab plane. As shown in the inset of Fig. 2(a), the Cr atoms are magnetically coupled through PO_4 chemical groups, with a nearest-neighbor Cr–Cr super-exchange path Cr–O–P–O–Cr.

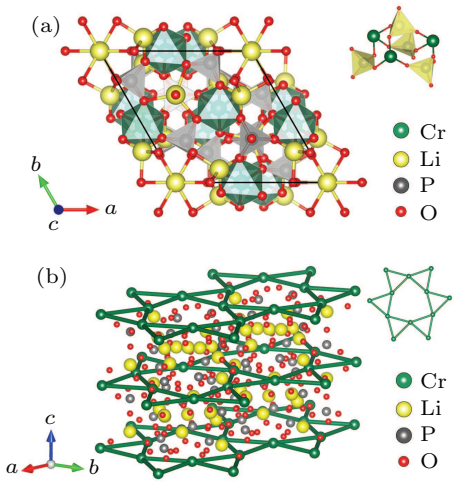


Fig. 2. Crystal structure of $Li_9Cr_3(P_2O_7)_3(PO_4)_2$: (a) crystal structure projected along the c-axis (polyhedron of Cr–O and P–O is highlighted). The inset demonstrates the magnetic coupling of Cr atoms through the PO_4 chemical group. (b) Schematic diagram of the magnetic structure emphasizing the corner-sharing triangular lattice made of Cr^{3+} (other atoms are omitted from the drawing for clarity in the inset).

3.2. Thermodynamic properties and phase diagram

In Fig. 3(a), we present the temperature dependence of the inverse magnetic susceptibilities $1/\chi$ under a field of 0.5 T. We perform a linear fit on the $1/\chi$–T data from 25 K to 100 K

using the Curie–Weiss law $\chi = C/(T-\theta)$, (where C is the Curie constant, and θ is the Curie–Weiss temperature), yielding θ values of approximately 5.8 K (for $B \parallel ab$-plane) and 5.5 K (for $B \parallel c$-axis), which provide insight into the ferromagnetic exchange coupling strength. Additionally, the effective magnetic moments $\mu_{\rm eff}$ of $Li_9Cr_3(P_2O_7)_3(PO_4)_2$ are approximately 3.8 $\mu_{\rm B}$ (for $B \parallel ab$-plane) and 3.85 $\mu_{\rm B}$ (for $B \parallel c$-axis), respectively.

In Fig. 3(b), we observe that at 1.8 K the saturation magnetization for $B \parallel ab$-plane and $B \parallel c$-axis is approximately 3.05 $\mu_{\rm B}$ and 3.11 $\mu_{\rm B}$ per Cr, respectively. Notably, the material reaches saturation faster when the magnetic field is parallel to the *ab*-plane, indicating that this material is an easy-plane ferromagnetic material, consistent with the findings reported by Akshata Magar *et al.*[17]

Figures 3(c) and 3(d) depict the temperature-dependent magnetization of $Li_9Cr_3(P_2O_7)_3(PO_4)_2$ with the magnetic field applied along different directions. These figures illustrate that $Li_9Cr_3(P_2O_7)_3(PO_4)_2$ undergoes a magnetic transition at around 2.7 K from the paramagnetic state to the ferromagnetic ordered state under a lower magnetic field (0.005 T) with the magnetic moment lying in the kagome plane. Interestingly, the test curves of zero field cooling (ZFC) and field cooling (FC) modes are not separated, indicating negligible hysteresis. The magnetic susceptibility under this condition is 43 (emu/mol) per Cr ($B \parallel a$-axis) and 3.5 (emu/mol) per Cr ($B \parallel c$-axis), respectively, which further supports the possibility that this material is an easy-plane material. Moreover, we apply a *c*-axis directional field to rotate the spin alignment from the kagome plane to the *c*-axis (as shown in Fig. 3(d)), and find that the magnetic transition temperature is reduced as we increase the field, prompting further exploration of its physical properties and field-induced magnetic phase diagram.

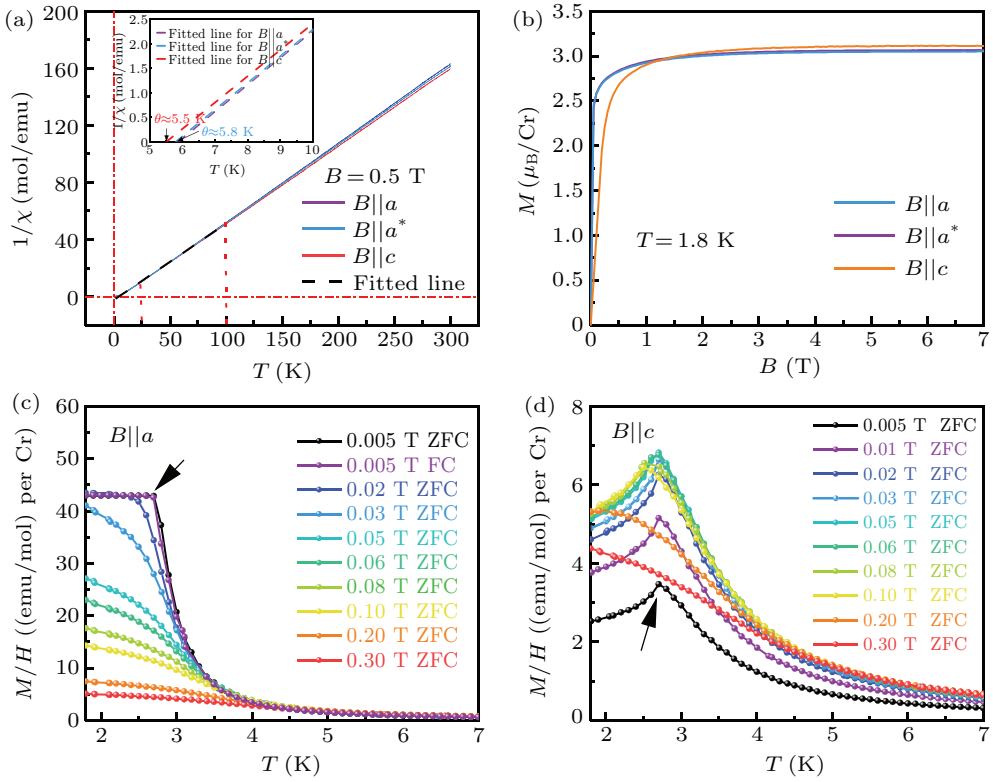


Fig. 3. Magnetic measurement of $Li_9Cr_3(P_2O_7)_3(PO_4)_2$ for applied magnetic fields along different directions: (a) temperature dependence of inverse magnetic susceptibility $1/\chi$ in three directions under a magnetic field of 0.5 T. The black dashed line is the fitting plot of Curie–Weiss law at low temperature (25–100 K). The inset shows the linear fit extended to intercept with $y = 0$ so it shows the Curie–Weiss temperatures intuitively. (b) Field-dependent magnetization of $Li_9Cr_3(P_2O_7)_3(PO_4)_2$ at 1.8 K. (c) Temperature-dependent magnetic susceptibilities for magnetic fields along the *a*-axis. Arrow indicates the transition temperature. (d) Temperature-dependent magnetic susceptibilities for magnetic fields along the *c*-axis. Arrow indicates the transition temperature.

To better understand the nature of the magnetic phase transition in $Li_9Cr_3(P_2O_7)_3(PO_4)_2$, we conducted measurements of specific heat in different directions under the influence of an external magnetic field. As depicted in Fig. 4(a), when the magnetic field is applied parallel to the *c*-axis, the magnetic phase transition of the sample occurs at $T = 2.7$ K. Notably, the characteristic peak of the phase transition gradually shifts to lower temperatures with increasing magnetic field strength when $B < 0.15$ T, while the crossover maximum shifts towards higher temperatures when $B > 0.2$ T. This indicates that $Li_9Cr_3(P_2O_7)_3(PO_4)_2$ exhibits characteristics of easy-plane ferromagnetic materials, where the internal magnetic moments experience spin reorientation as the external magnetic field increases along the *c*-axis.

Figure 4(b) shows that the magnetic phase transition occurs at $T = 2.7$ K when the magnetic field is applied parallel to

the *ab*-plane of $Li_9Cr_3(P_2O_7)_3(PO_4)_2$. Below this critical temperature, the material exhibits a ferromagnetic state, whereas above it, the state is paramagnetic. As the magnetic field increases, the crossover temperature maximum gradually shifts to higher temperatures, which is a characteristic feature of a ferromagnetic transition.

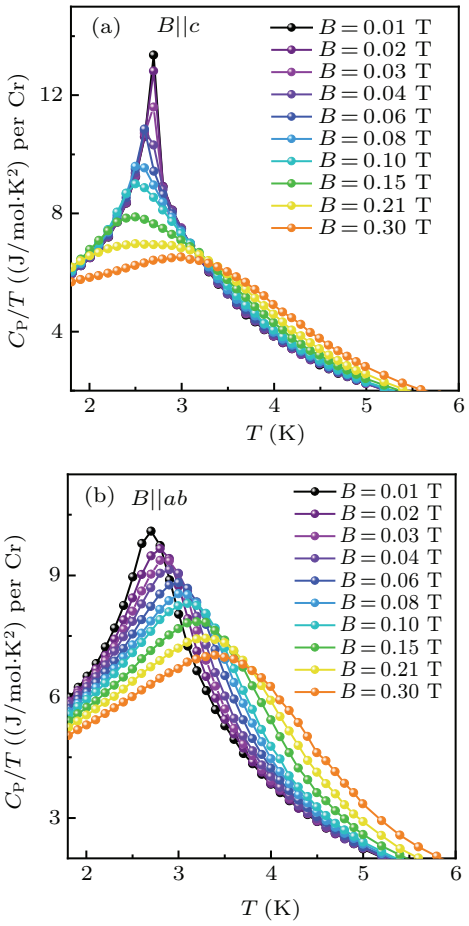


Fig. 4. The C_P/T for $Li_9Cr_3(P_2O_7)_3(PO_4)_2$ with selected fields along the *c*-axis in (a) and the *ab*-plane in (b).

For $Li_9Cr_3(P_2O_7)_3(PO_4)_2$, we have constructed a phase diagram that depicts the critical behavior of the material and sheds light on the underlying mechanisms. To investigate the magnetic phases induced by fields applied along the *c*-axis, we measured the magnetic-field dependence of the magnetization M at various temperatures for $B \parallel c$ (as shown in Fig. 5(a)). By differentiating the M–B curve, we identified critical points (indicated by arrows in the inset of Fig. 5(a)) that mark the saturation field for magnetic phase transitions from the easy-plane ferromagnetic state to the fully polarized state. The second derivative magnetization curves of $Li_9Cr_3(P_2O_7)_3(PO_4)_2$ for $B \parallel c$, shown in the inset of Fig. 5(a), reveal the peak positions that determine the saturation field. We selected critical points in the M–B curve (Fig. 5(a)), M–T curves (Fig. 3(d)), and C_P/T–T curves (Fig. 4(a)) to construct the magnetic phase diagram presented in Fig. 5(b). We note that the phase boundary in our phase diagram is linear over a certain temperature range between 1.8 K and 2.5 K.

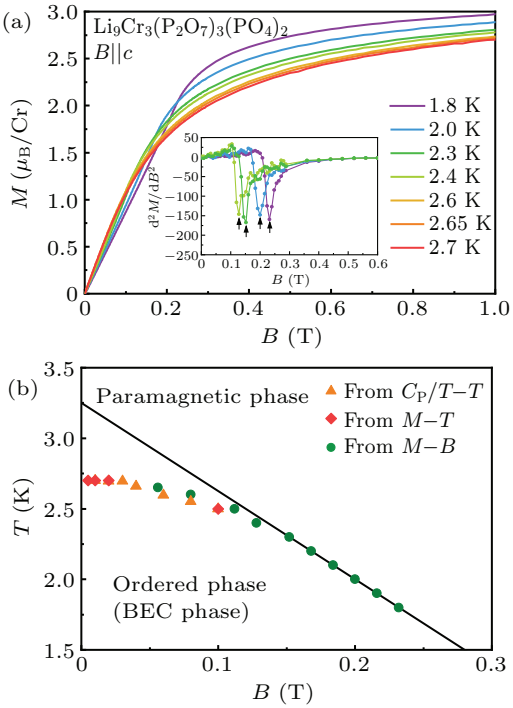


Fig. 5. (a) Magnetic-field dependence of the magnetization M in $Li_9Cr_3(P_2O_7)_3(PO_4)_2$ measured at various temperatures for $B \parallel c$. The inset is the second derivative magnetization curves at selected temperatures and arrows indicate the transition fields $H(T)$. (b) The phase diagram of temperature vs. internal magnetic field for $Li_9Cr_3(P_2O_7)_3(PO_4)_2$ with $B \parallel c$.

The magnetic transition of the spin reorientation in the easy-plane ferromagnet can be understood as a magnon Bose–Einstein condensation, as proposed by Syromyatnikov.[15] The dimensionality of the BEC transition is characterized by the critical exponent, which relates the transition boundary scaling to $|H_C(T) - H_C(0)| \propto T^{\phi}$ with $\phi = d/2$, where d is the system dimension (d is equal to 3 in a 3D system and 2 in a 2D system). For weakly coupled layered materials, where the temperature is higher than the interlayer coupling, the system can be approximated as a quasi-2D system.

In our system, we find that the phase boundary scales linearly with temperature, indicating a quasi-two-dimensional magnon BEC, similar to the quasi-2D ferromagnetic magnon BEC observed in the material K_2CuF_4.[16]

4. Conclusion

Our research on $Li_9Cr_3(P_2O_7)_3(PO_4)_2$ adds to the growing body of knowledge on the magnetic properties of kagome materials, and highlights the potential for further investigation of this family of materials. Our findings suggest that $Li_9Cr_3(P_2O_7)_3(PO_4)_2$ is an easy-plane kagome ferromagnet with $S = 3/2$ and a ferromagnetic exchange coupling strength, and undergoes a magnetic transition from a paramagnetic to a ferromagnetic state at $T_C = 2.7$ K. The field-induced phase transition observed in our study is consistent with the theory of

quasi-2D magnon Bose–Einstein condensation, and the constructed phase diagram provides valuable insights into the behavior of this material under external magnetic fields.

While our study has provided important results, there is still much to be explored in this system. For example, a transition from quasi-2D BEC to a 3D BEC may be observed when the temperature is lower than the interlayer interaction. Future research could aim to obtain more accurate data at lower temperatures of $Li_9Cr_3(P_2O_7)_3(PO_4)_2$. Overall, our work on $Li_9Cr_3(P_2O_7)_3(PO_4)_2$ opens up new avenues for investigation in this fascinating family of materials.

Acknowledgement

Project supported by Shenzhen Fundamental Research Program (Grant No. JCYJ20220818100405013).

References

[1] Meschke V, Gorai P, Stevanovic V and Tober E S 2021 *Chem. Mater.* **33** 4373

[2] Nytko E A, Helton J S, Müller P and Daniel G N 2008 *J. Am. Chem. Soc.* **130** 2922

[3] Feng Z, Li Z, Meng X, Yi W, Wei Y, Zhang J, Wang Y C, Jiang W, Liu Z, Li S Y, Liu F, Luo J L, Li S L, Zheng G Q, Meng Z Y, Mei J W and Shi Y G 2017 *Chin. Phys. Lett.* **34** 077502

[4] Okamoto Y, Nohara M, Aruga-Katori H and Takagi H 2007 *Phys. Rev. Lett.* **99** 137207

[5] Poisson S, d'Yvoire F, Bretey E and Berthet P 1998 *J. Solid State Chem.* **138** 32

[6] Gao H, Zhang S and Deng C 2015 *Dalton Trans.* **44** 138

[7] Xu J, Zhao Y and Kuang Q 2011 *J. Sol-Gel Sci. Technol.* **59** 521

[8] Kermarrec E, Kumar R, Bernard G, Henaff R, Mendels P, Bert F, Paulose P L, Hazra B K and Koteswararao B 2021 *Phys. Rev. Lett.* **127** 157202

[9] Balasubramanian P, Mancini M, Geßwein H, Geiger D, Axmann P, Kaiser U and Mehrens M W 2018 *ChemElectroChem* **5** 201

[10] Yao H, Chen D, Zhang J, Duan H, Chen M, Zhou Z Y, Zhao Y M, Kuang Q, Fan Q H and Dong Y Z 2021 *J. Solid State Electrochem.* **25** 2267

[11] Onoda M and Takada S 2019 *J. Phys. Soc. Jpn.* **88** 034709

[12] Onoda M and Takada S 2019 *J. Phys. Soc. Jpn.* **88** 064003

[13] Onoda M and Takada S 2020 *J. Phys. Soc. Jpn.* **89** 034002

[14] Onoda M and Takada S 2020 *J. Phys. Soc. Jpn.* **89** 074002

[15] Syromyatnikov A V 2007 *Phys. Rev. B* **75** 134421

[16] Satoshi S, Kurita N, Yamada M and Tanaka H 2017 *Phys. Rev. B* **95** 174406

[17] Magar A, Somesh K, Singh V, Abraham J, Senyk Y, Alfonsov A, Büchner B, Kataev V, Tsirlin Aand Nath R 2022 *Phys. Rev. Appl.* **18** 054076

[18] Capitelli F, Dridi N, Arbib E H, Valentini V and Mattei G 2007 *Z. Kristallogr.* **222** 521

[19] Luo Y, Gu F, Shui M and Shu J 2019 *Ionics* **25** 5689